Delft University of Technology

Acoustic measurements of a DU96-W-180 airfoil with flow-misaligned serrations at a high Reynolds number in a closed-section wind tunnel

Merino Martinez, Roberto; van der Velden, Wouter; Avallone, Francesco; Ragni, Daniele

Important note
To cite this publication, please use the final published version (if applicable).
Please check the document version above.

Acoustic measurements of a DU96-W-180 airfoil with flow-misaligned serrations at a high Reynolds number in a closed-section wind tunnel

**Roberto Merino-Martinez, Wouter van der Velden, Francesco Avallone & Daniele Ragni,
Faculty of Aerospace Engineering, Delft University of Technology, Kluyverweg 1, 2629 HS, Delft, the Netherlands.
Email: r.merinomartinez@tudelft.nl**

Summary

Trailing-edge serrations are passive noise reduction add-ons widely used in wind-turbine applications. This study presents acoustic beamforming results of microphone array measurements of a cambered airfoil (DU96-W-180) in a closed-section wind-tunnel at a Reynolds number of industrial interest. Two different serration geometries with different lengths were tested and compared with the straight-edge baseline airfoil. The serrations were set at a flap angle of 6 degrees. Several flow velocities and angles of attack were tested at three chord-based Reynolds numbers ranging from 5×10^5 to 1.5×10^6. A phased microphone array was used to obtain source maps of the trailing-edge noise; Particle Image Velocimetry (PIV) was employed to obtain information about the turbulent boundary layer approaching the trailing edge; further, a numerical simulation using the Lattice Boltzmann Method (LBM) was performed for comparison. Far-field noise from the experimental data and computations shows a satisfactory agreement. Noise reductions of several dB were obtained, especially at lower frequencies. An increase in high-frequency noise is observed after a crossover frequency, which is assumed to be due to the set flap angle.

1.   Introduction

Noise emission from wind turbines is one of the main issues that the wind energy industry currently must deal with. The power production of a single wind turbine is limited by strict noise regulations: a decrease of 1 dB of the sound pressure level (SPL) is expected to raise the energy production by 2 to 4% (Oerlemans and Fuglsang, 2012).

Trailing-edge serration is the most used passive noise reduction device to reduce turbulent boundary layer trailing-edge noise of wind turbine blades (Oerlemans 2016). The most common design features thin, solid, sawtooth patterns attached to the trailing edge (Gruber et al., 2011).

Previous researches focused on symmetric airfoils in an open-jet wind tunnel, such as NACA 0018 wings with retrofitted serrations with and without flap angle (Arce León et al., 2016a; 2016b; Avallone et al. 2016). Noise reductions of about 6 dB were measured for different flow speeds. In addition, a comparison with numerical simulations showed satisfactory agreement (van der Velden and Oerlemans, 2017). The low Reynolds numbers usually obtainable in open jet facilities and ambiguities in the definition of the angle of attack, due to the flow expansion, limit their industrial utilization. On the other hand, closed-section wind tunnels provide a well-characterized aerodynamic flow, further improving the comparison with numerical simulations (Pagani et al., 2016), but less accurate acoustic measurements. The latter are

affected by the typical high background noise levels, the convection of the sound waves due to the air flow, reflections on the tunnel walls, and the interaction of the turbulent boundary layer of the wind tunnel with the microphones, if these are installed flush-mounted on the wall of the tunnel. In order to alleviate these effects, phased microphone arrays and beamforming algorithms are usually adopted to estimate the location and strength of sound sources (Mueller, 2002).

This study investigates the noise emissions of a cambered airfoil (DU96-W-180) in a closed-section wind tunnel at Reynolds numbers of industrial interest. A straight trailing-edge baseline case and two different serration geometries with flap angle are studied.

Microphone array measurements were performed to measure the noise emissions at the trailing edge of each configuration. Particle Image Velocimetry (PIV) measurements provided information about the boundary layer characteristics at the trailing edge. In addition, computational simulations using the Lattice Boltzmann method were performed to compare and assess the accuracy of the experimental far-field acoustic measurements.

The current paper is structured as follows: Section 2 describes the methodology, i.e., the beamforming algorithm and the computational method. The experimental setup and the model geometry are introduced in Section 3. Section 4 shows the experimental results and the comparison with computations. Finally, Section 5 summarizes the manuscript.

2. Methodology

2.1 Beamforming method

The application of beamforming algorithms to the acoustic data recorded by a phased microphone array allows for the estimation of the location and strength of sound sources (Johnson and Dudgeon, 1993; Merino-Martinez et al., 2016; Malgoezar et al., 2017). A scan grid needs to be defined, where each grid point is considered as a potential sound source.

Conventional frequency domain beamforming (Johnson and Dudgeon, 1993) was employed in this study, since it is a robust, simple and fast algorithm. The convection of the sound waves was considered in the formulation (Sijtsma, 2010). Since this method is based on single point sources, an additional integration method, more suitable for distributed noise sources, is used. It consists in integrating over an area of interest and normalizing the result by the integrated array response function (Sijtsma and Stoker, 2004; Sijtsma, 2010). In this paper, an integration method similar to the Source Power Integration technique (Sijtsma, 2010), which considers a covariance matrix fitting (Yardibi et al., 2010) based on the assumption of a line source, was applied over a region of the source map obtained by conventional beamforming (see section 3.2). This method was recently proposed by Sijtsma (Sijtsma, 2016) and was proven to provide very accurate results in the microphone array methods benchmark (Sarradj, 2017) for a simulated linear sound source, heavily contaminated with background noise, which resembles the measurement of trailing-edge noise in a closed-section wind tunnel.

In order to obtain the sound frequency spectrum of the integration area with this method, the following formula is applied for each frequency of interest:

$$A(f) = \frac{\sum_{j=1}^{K}\left(\boldsymbol{g}_j^* \boldsymbol{C}_{exp} \boldsymbol{g}_j\right)}{\sum_{j=1}^{K}\left(\boldsymbol{g}_j^* \boldsymbol{C}_{sim} \boldsymbol{g}_j\right)} \tag{1}$$

where an asterisk ($*$) denotes the complex conjugate transpose, f is the frequency, $\boldsymbol{g}_j$ is the steering vector for the jth grid point in the integration area (Sijtsma, 2010), $\boldsymbol{C}_{\text{exp}}$ is the cross-spectral matrix obtained from the experimental measurements and $\boldsymbol{C}_{sim}$ is the simulated cross-spectral matrix due to the considered line source (using the same microphone distribution). In this case, the line source was assumed to be in the airfoil trailing-edge position. Both summations in Equation (1) apply to the K grid points within the integration area considered.

Performing acoustic measurements in closed wind tunnel test sections is a challenging task (Mueller, 2002; Pagani et al., 2016) as described earlier. Therefore, the main diagonal of the cross-spectral matrix of the Fourier-transformed microphone signals was removed to suppress the effect of incoherent noise (mostly due to the wind tunnel boundary layer interaction with the microphones) and improve the beamforming results (Sijtsma, 2010). Since this technique might cause inaccuracies in the absolute source strength, in the following only the relative differences between values corresponding to different configurations are reported because of their higher reliability (Oerlemans and Sijtsma, 2004).

A similar aeroacoustic experiment is presented in (Pagani et al., 2016) where slat noise was measured, instead of trailing-edge noise. The advanced deconvolution method DAMAS (Brooks and Humphreys, 2006) provided similar source distributions and integrated sound spectra as conventional frequency domain beamforming.

2.2 Lattice Boltzmann method (LBM)

The commercial software package Exa PowerFLOW 5.3c was used to solve the discrete Lattice‑Boltzmann equations for a finite number of directions. For a detailed description of the equations used for the source field computations the reader can refer to (Succi, 2001) or (van der Velden et al., 2016). Here, only summary is presented regarding the computational method.

The discretization used for this application consisted of 19 discrete velocities in three dimensions (D3Q19) involving a third‑order truncation of the Chapman‑Enskog expansion, which is suitable and give accurate results for low Mach number flows. The distribution of particles was solved using the kinetic equations on a Cartesian mesh, with the Bhatnagar‑Gross‑Krook (BGK) collision term operator (Bhatnagar et al., 1954). A Very Large Eddy Simulation (VLES) was implemented as viscosity model to locally adjust the numerical viscosity of the scheme (Chen et al., 2003). The model consists of a two‑equation k‑ε Renormalization Group (RNG) modified to incorporate a swirl based correction that reduces the modeled turbulence in presence of large vortical structures. A turbulent wall‑model was used to resolve the near‑wall region (Chen and Doolen, 1998). The choice of the model allowed to obtain a reliable estimate of the boundary layer till the viscous sub‑layer, with feasible turn‑around times. The surface itself is modelled by a cut-cell approach, which avoids meshing complex geometry. Especially for the current application, where the flow around complex sawtooth trailing edges have to be solved, this is a huge advantage over other computational methods.

Since the LBM is inherently compressible and it provides a time‑dependent solution, the sound pressure field was extracted directly from the computational domain. Sufficient accuracy is obtained when considering at least 16 cells per wavelength for the LBM (Habibi et al., 2013). The obtained far‑field noise was further compared with noise estimated by using an acoustic analogy. For this purpose, the Ffowcs‑Williams and Hawkings (FWH) (Williams and Hawkings, 1969) equation was employed. The time‑domain FWH formulation developed by Farassat (Farassat and Succi, 1980) was used to predict the far‑field sound radiation of the serrated

trailing edge in a uniformly moving medium (Brès et al., 2010). The input to the FWH solver is the time‑dependent pressure field of a surface mesh provided by the transient LB simulations.

3.   Experimental setup

3.1 Model geometry

The experiments were performed at the Delft University of Technology Low Turbulence Wind Tunnel (LTT). This wind tunnel has a contraction ratio of 17.8 and the freestream turbulence level in the test section varies from 0.04% at 20 m/s to 0.1% at 75 m/s.

The tunnel has an octagonal closed test section 1.8 m wide, 1.25 m high and 2.6 m long. A DU96-W-180 airfoil with a span of 1.25 m and a chord of 0.6 m was vertically installed flush-mounted to the tunnel section (Figure 1) and tested at different flow speeds (U$_\infty$ = 12.4, 24.8 and 37.4 m/s) and angles of attack, (α = -6, -2, 0, 2, 6, 9 and 12 degrees). These flow speeds were chosen to result in a chord-based Reynolds numbers of 5×10^5, 10^6 and 1.5×10^6 and Mach numbers of 0.037, 0.073, and 0.11, respectively.

Three different trailing-edge geometries were investigated: a straight edge (which is considered as a baseline configuration), and two sawtooth serrations of different lengths (l): the Sr05 configuration with l equal to 5% of the airfoil chord (3 cm) and the Sr15 with l equal to 15% of the airfoil chord (9 cm). The width of both sawtooth serrations is half of the length, i.e., 1.5 cm and 4.5 cm, respectively (Figure 2). These serration geometries are based on a boundary layer thickness of 3 cm at the suction side, obtained with XFOIL calculations under similar flow conditions, and, in addition, confirmed by Devenport et al. (2010). The serrations were manufactured by laser cutting a steel flat plate with a constant thickness of 1.5 mm and retrofitted to the trailing edge keeping the surface free from irregularities. Both serrations were set at a flap angle of $\phi = 6$ degrees.

The coordinate system adopted in the manuscript is reported in Figure 1. The x axis is oriented in the downwind streamwise direction, the z axis in the vertical direction and the y axis perpendicular to the xz plane and it points at the microphone array. The origin of this coordinate system is located at the midspan of the airfoil.

Computations were performed on the same model geometry under similar flow characteristics. The same coordinate system is used. For the sake of conciseness, only results for chord-based Reynolds number equal to 1.5×10^6 (U$_\infty$ = 37.4 m/s) and angle of attacks of -2 degrees (zero-lift angle for this airfoil) and 6 degrees are presented in this paper. Transition from laminar to turbulent in these conditions is natural as in the experiments. The computational domain is 20 chord lengths long (12 m) in the x and y directions while it is equal to the span of the model (1.25 m) in the z direction. The outer region holds an anechoic layer to damp out the acoustic waves near the far-field boundaries. Spanwise cyclic boundary conditions are applied at the edge of the model span. At the inlet a fixed velocity is described, and the outlet is modeled by fixing the static pressure, while maintaining a free flow direction. The simulated Mach number is identical to the real Mach number, i.e., 0.11. The grid used in this study has 60,000,000 voxels, with 8 different refinement regions located around the airfoil. The finest voxels, around the straight and serrated trailing edges, are cubes of size 3.52 x 10^{-4} m considered sufficient to correctly capture the most relevant features of the boundary layer and the near wake. The boundary layer was modeled using the inbuilt wall model, with the closest cell located around y^+ = 50. The Courant-Friedrichs-Lewy (CFL) stability number was set to unity by the solver, to ensure stable conditions. Simulations were run for a physical time of 0.3 s (approximately 20 flow passes). A total of 10 flow passes were used for detailed analysis. Statistical data was recorded at a frequency of 26 kHz, and used for a prediction of the acoustic far-field noise. For

each 0.1 s of physical time (6.5 flow passes), 450 CPU hours were necessary on a Linux Xeon E5-2690 2.9 GHz platform with 20 cores.
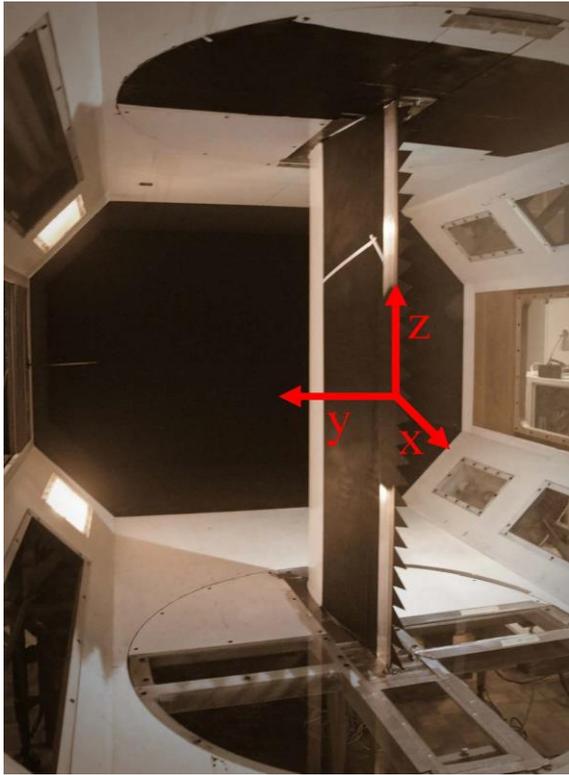
Figure 1 - Wind tunnel setup and airfoil model.
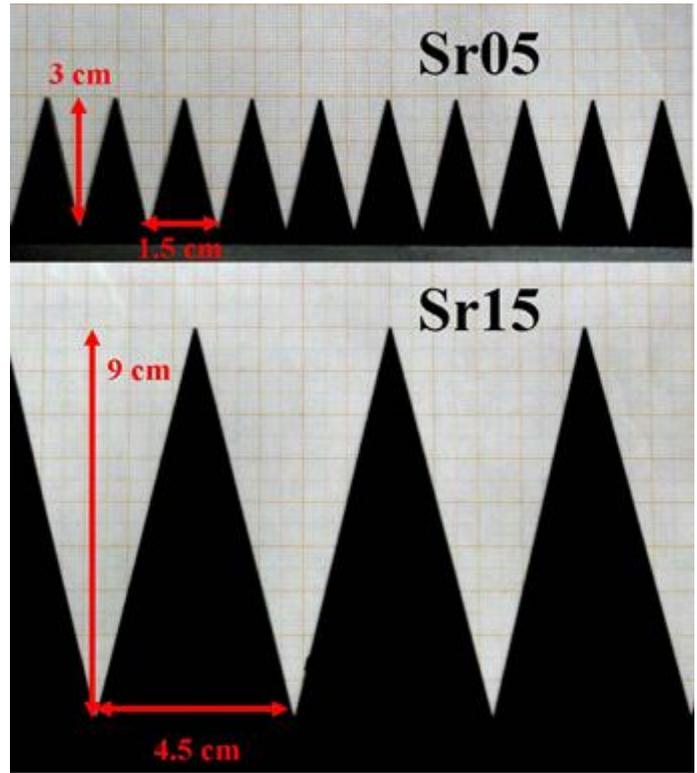
Figure 2 – Trailing-edge serration geometries.

3.2 Acoustic measurements

A phased microphone array was installed with recessed microphones. Recession was about 2 cm deep and had an opening angle of 60 degrees. Microphones were installed along one of the walls of the wind tunnel behind an acoustically-transparent flat Kevlar window (see Figure 3). The setup configuration allows to keep the closed test section configuration alleviating the effect of the turbulent boundary layer convecting along the wall.

The array consisted of 64 microphones in a multi-arm logarithmic spiral distribution with an elliptical shape with a mayor axis of 0.93 m, see Figure 4. The distance from the array to the scan plane (i.e., the airfoil trailing-edge position) was 0.9 m and it was facing the suction side of the airfoil. The center microphone at the array was aligned with the middle point of the trailing edge (for the case with $\alpha = 0°$).

Data was acquired for 30 s at a sampling frequency of 50 kHz. The acoustic data was averaged using time blocks of 2048 samples (Δt = 40.96 ms) for each Fourier transform and windowed using a Hanning weighting function with 50% data overlap. With these parameters, the frequency resolution is 24.4 Hz and the expected error (Brandt, 2011) in the cross-spectrum estimate is 3.7%. Unfortunately, no background noise measurements with the empty tunnel could be performed, so the signal to noise ratio is not known.

The scan grid for beamforming covered the expected area of noise generation, ranging from $x = -1\,m$ to $x = 0.5\,m$ and from $z = -0.65\,m$ to $z = 0.65\,m$ with a separation between grid points of 1 mm, see Figures 5 and 6. Therefore, the considered grid size was 1501×1301.

Figure 3 - Kevlar window (in yellow) in one of the LTT wind tunnel walls.
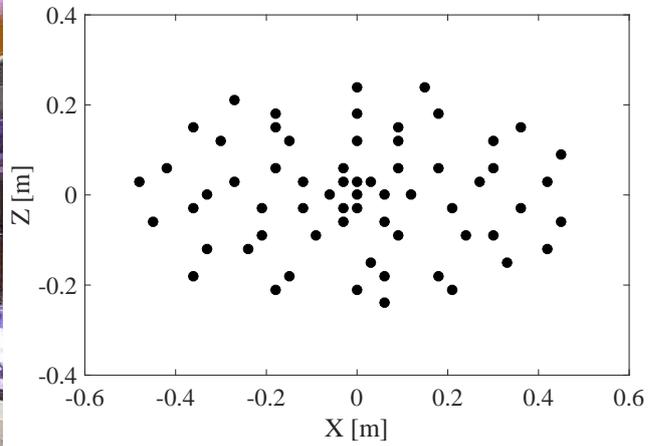
Figure 4 - Microphone array distribution. Coordinates are given in the airfoil system.

The integration area for the application of the method described in section 2.1 extended from $x = -0.1\ m$ to $x = 0.1\ m$ and from $z = -0.5\ m$ to $z = 0.5\ m$ (see the dashed lines in Figures 5 and 6). This region covered the whole serration length for both geometries and prevented possible contaminations from wind tunnel boundary layer interactions with the model ends (corner sources) (Tuinstra and Sijtsma, 2015) and other noise sources while still providing spanwise statistically meaningful results of the trailing-edge noise (Pagani et al., 2016).

3.3 PIV measurements

Stereoscopic PIV experiments were conducted to measure the three-component velocity fields in planes perpendicular to the serration surface at the trailing edge of the wing. The required illumination was provided by a Quantel Evergreen Nd:YAG laser system with an average output of 200 mJ/pulse. The laser light was conveyed to form a 2 mm laser sheet of about 0.3 m width at the field of view. Two LaVision Imager Pro LX 16 Mpix (4870 × 3246 px, 12 bits, pixel pitch of 7.4 µm/px) were used. They were equipped with two Nikon lenses of focal length f = 200 mm and set at an aperture f# = 2.8 – 4. They were set at about 40 degrees angle at about 1 m distance from the model. The resulting field of view was 100 × 140 mm^2. The magnification factor was M = 0.25 resulting in a digital resolution of approximately 34 px/mm. The focusing plane was slightly offset with respect to the laser plane (defocusing), to obtain an image of the particle of about 2.3 px. Therefore, no bias error due to peak-locking is expected (Westerweel, 1997). Seeding was provided in the test section by a SAFEX smoke generator with SAFEX MIX, able to produce liquid droplets of less than 1 µm. Ensembles of 1000 uncorrelated double-frame recordings per dataset were acquired and processed by LaVision Davis 8.1.4. Particle images were processed using final interrogation windows of 24 × 24 px with 75% overlap resulting in a vector spacing of 0.18 mm. The main PIV parameters are gathered in Table 1.

4.   Results

4.1 Beamforming source plots

Examples of the beamforming source plots are presented in Figures 5 and 6, where the acoustic images for the three airfoil configurations (straight trailing edge, short serrations Sr05 and long serrations Sr15) are shown for the one-third octave bands of 2 and 4 kHz, respectively. Both figures refer to an angle of attack of 6 degrees and U_∞ = 37.4 m/s corresponding to a Reynolds number of 1.5×10^6.

Table 1 – PIV parameters

Parameters		Stereoscopic PIV setup	
Measurement field of view	FOV	100 × 140 mm^2	4870 × 3246 px^2
Interrogation window size	Iw	0.72 × 0.72 mm^2	24 × 24 px^2
Vector spacing	S	0.18 mm	6 px
Digital resolution	DR	~34 px/mm	
Magnification	M	0.25	
Vectors	NV	538 × 769	
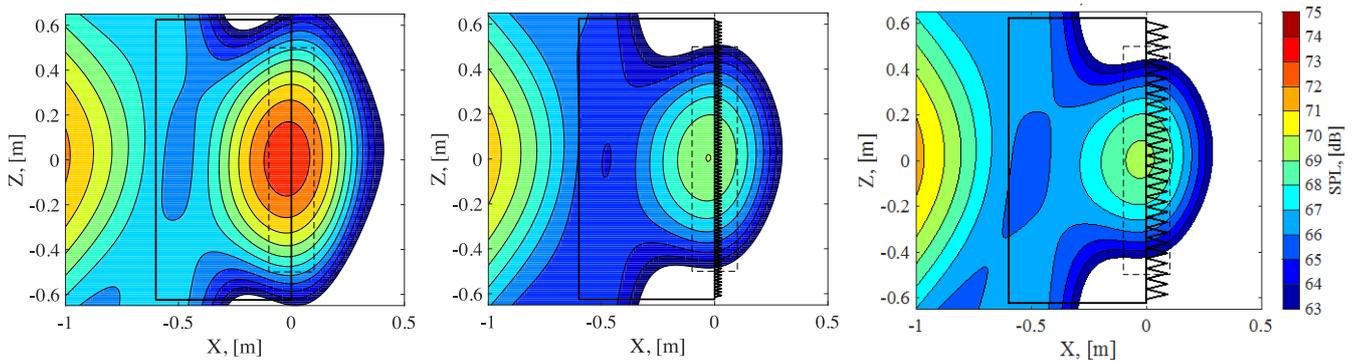
Figure 5 – One-third octave band (2 kHz) beamforming source plot for the straight trailing edge (left), short serrations (center) and long serrations (right) with U$_\infty$ = 37.4 m/s, α = 6 degrees and Re = 1.5×10^6. The solid black line represents the airfoil position and the dashed black line, the integration area.
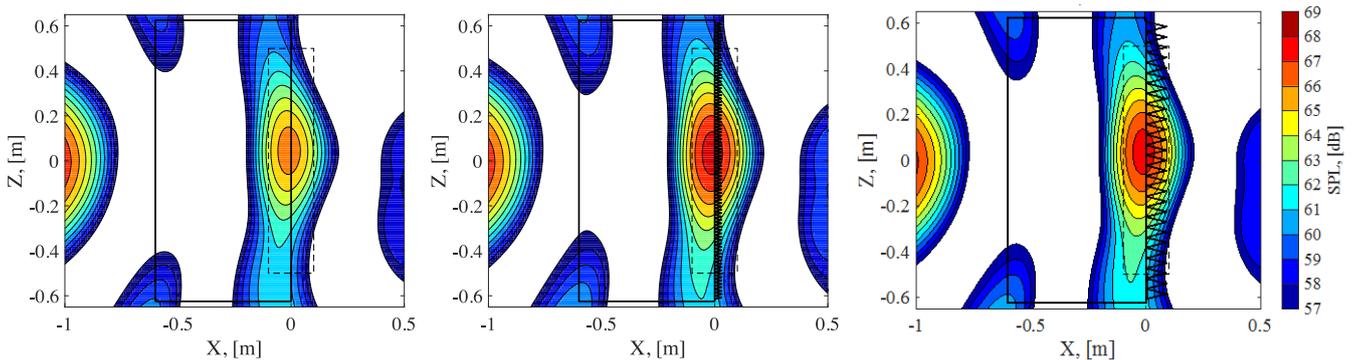
Figure 6 - One-third octave band (4 kHz) beamforming source plot for the straight trailing edge (left), short serrations (center) and long serrations (right) with U$_\infty$ = 37.4 m/s, α = 6 degrees and Re = 1.5×10^6. The solid black line represents the airfoil position and the dashed black line, the integration area.

In Figure 5, trailing-edge noise reductions ($\Delta\phi_{aa}$ in Figures 8 and 9) (considering the peak values in the image) with respect to the straight edge baseline of around 3 dB and of 4 dB are measured for the short and long serrations respectively. As previously mentioned, the integration of the source map over an area (marked with a dashed black line) prevents to some extent the inclusion of unwanted noise sources, such as leading edge noise or noise sources present in the wind tunnel itself. This type of sources can also be seen in Figures 5 and 6.

In Figure 6, on the other hand, it is seen that the short serrations show noise increase (considering peak values) of around 3 dB and 2 dB for the short and long serrations, respectively. The three plots in Figure 6 show two corner sources on the junctions of the leading edge with the tunnel wall, most probably due to the interaction of the boundary layer of the wind tunnel with the model.

The noise reductions observed by the serrated trailing edges agree with those obtained in Oerlemans et al., 2009 in field measurements on full-scale wind turbines, where a noise increase after a crossover frequency was also noticed.

4.2 PIV results

In order to compare computations and experiments, boundary layer profiles at 95% of trailing-edge suction side are investigated for the baseline straight trailing edge case. In Figure 7, both mean ($\bar{u}$) and rms ($\overline{u'}$) streamwise velocity are depicted for $\alpha = -2$ degrees and $\alpha = 6$ degrees. For $\alpha = -2$ degrees (Figure 7 (a) and (b)), the turbulent boundary layer results are very similar for the two methods, both in terms of mean and fluctuating velocity. Excellent agreement is found between PIV and LBM. On average, a boundary layer thickness of δ = 13 mm is found, with a shape factor of H = 1.5, indicating a fully developed turbulent boundary layer.

The mean boundary layer of the $\alpha = 6$ degrees case (Figure 7 (c)) is slightly different close to wall, when comparing PIV and LBM. Due to the cambering of the DU96-W180 airfoil, and therefore the stronger adverse pressure gradient, transition seems to be delayed in the experiment, resulting in a less turbulent boundary layer. The boundary layer thickness was measured to be δ = 21 mm, with a shape factor of 1.9. In the simulated results, the boundary layer behaves differently, although the fluctuations are captured adequately. This deviation could also explain the larger differences between the far-field reduction results for this case, presented in subsection 4.3.

(a) (b) (c) (d)
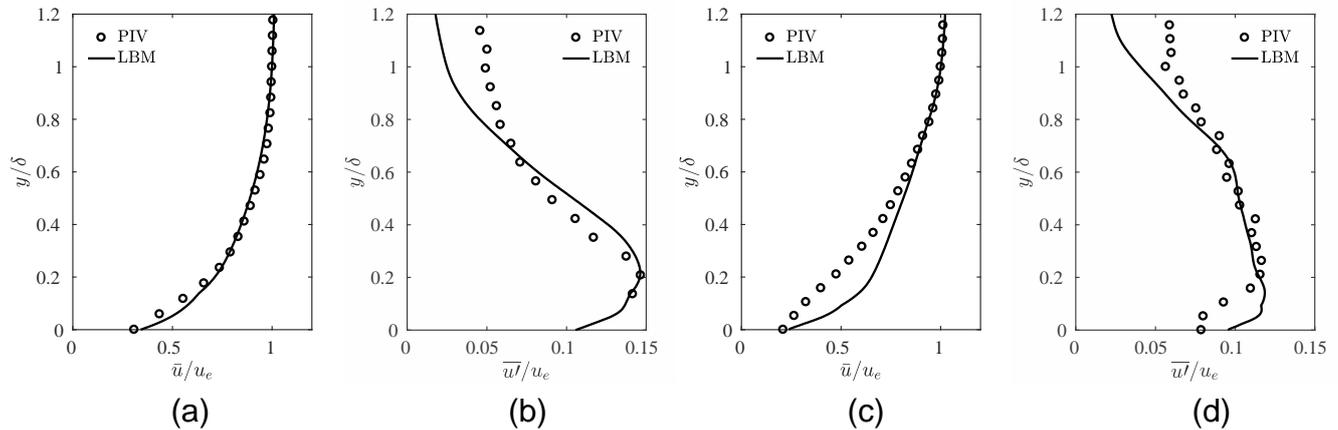
Figure 7 – Boundary layer characteristics from both PIV and LBM obtained at 95% of the baseline trailing-edge suction side. Normalized streamwise mean and rms velocity for $\alpha = -2$ degrees (a and b) and $\alpha = 6$ degrees (c and d).

4.3 Noise reduction comparison

The noise reductions ($\Delta\phi_{aa}$) achieved by both serrated geometries with respect to the straight trailing-edge baseline case are presented in Figure 8 for $\alpha = -2$ degrees and in Figure 9 for $\alpha = 6$ degrees, for a chord-based Reynolds number of $1.5{\times}10^6$ (U_∞ = 37.4 m/s). Positive values mean noise reduction. Both the results obtained by the integrated beamforming source plots and the LBM simulations are plotted in the same figure and show similar levels and trends for the selected frequency range (500 – 5,000 Hz). The reason for limiting the analysis to this frequency range is it is the region of highest confidence for both the acoustic measurements and LBM.

It can be observed in Figure 8 that reductions up to 5 dB are obtained for the short serrations and approximately of 4 dB for the long serrations between 1 and 2 kHz approximately. Since the long serrations have length approximately equal to 5 times the boundary layer thickness, minor increase in noise reduction are expected (Gruber et al., 2011).

The general trend shows that the noise reduction performance of the serrations worsens with increasing frequency, leading even to some noise increase after a crossover frequency of

approximately 3,800 Hz for both serration geometries. This is supposed to be due the flap angle of the serrations ($\phi = 6$ degrees) (Arce León et al., 2016b). Good agreement is found between experiment and simulation, giving confidence to both proposed methodologies in the paper. In addition, the noise reduction values obtained are of the same order of magnitude as those observed in (Gruber et al., 2011) for a similar experiment.
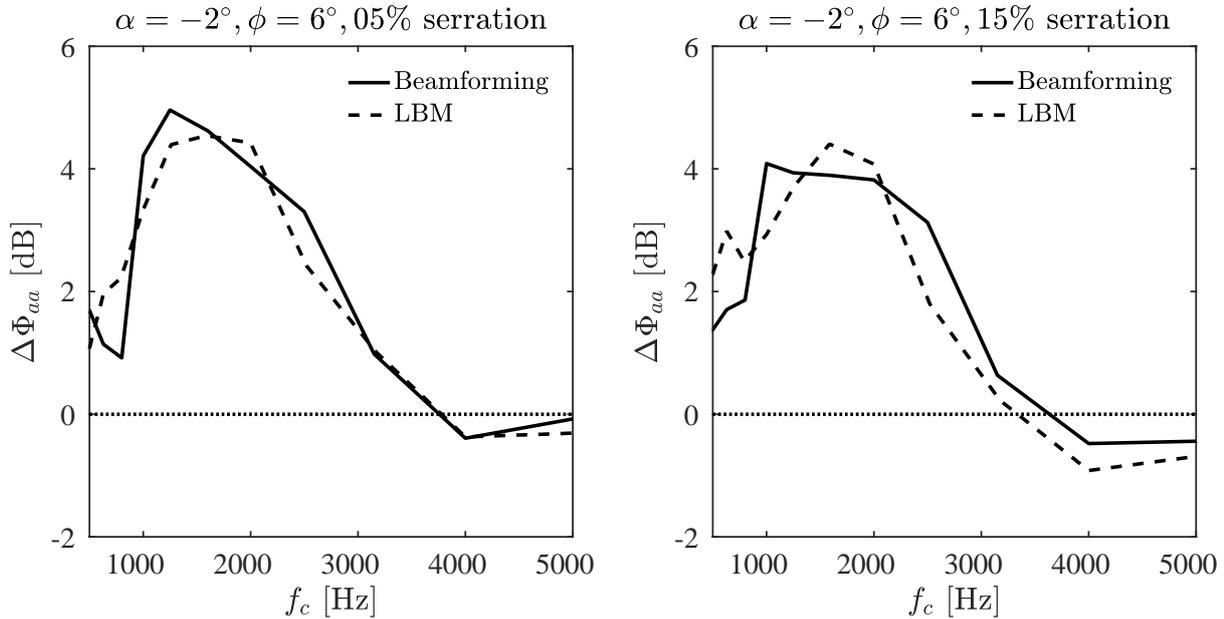
Figure 8 – Relative noise reductions obtained by the short serrations (left, Sr05) and the long serrations (right, Sr15) with respect to the baseline case for U∞ = 37.4 m/s, $\alpha = -2$ degrees. Both the experimental (solid line) and LBM (dashed line) results are compared. Positive values represent noise reductions.
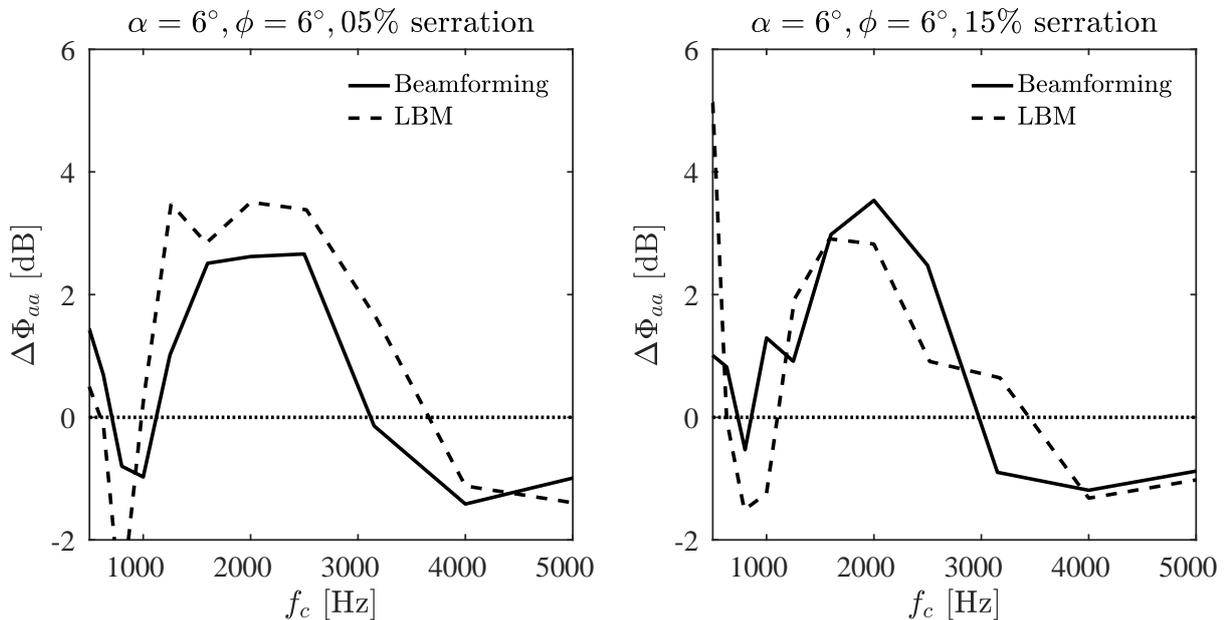
Figure 9 – Relative noise reductions obtained by the short serrations (left, Sr05) and the long serrations (right, Sr15) with respect to the baseline case for U∞ = 37.4 m/s, $\alpha = 6$ degrees. Both the experimental (solid line) and LBM (dashed line) results are compared. Positive values represent noise reductions.

In Figure 9 ($\alpha = 6$ degrees), similar trends as in Figure 8 can be observed, although with lower values for the whole spectrum, reaching maximum reductions of around 3 dB for both serrated geometries. Once again, a noise increase of around 1 dB is observed after a crossover frequency. This time the threshold frequency shows lower values, closer to 3 kHz. For $\alpha = 6$ degrees, also a cross-over frequency at the lower frequency is detected, around 800-1000 Hz. This behaviour is different to the behaviour observed in previous studies with symmetric airfoils

(Arce León et al., 2016a). The general agreement between experiment and simulation for $\alpha = 6$ degrees is worse, which could indicate a variation in the flow behaviour.

The noise reduction values obtained from the integrated beamforming results differ from those obtained by simply considering the peak values of the source plots in section 4.1. This confirms that the selected integration method is more suitable for line sources.

4.4 Directivity plots

In addition, the LBM computations provide the sound radiation directivity of the trailing-edge noise. Figure 10 presents the radiation directivity plots for the three configurations at ten chords distance for the case of $\alpha = -2$ degrees and Re = 1.5×10^6, banded in three different frequency ranges: 500-1,000 Hz, 1,000-2,000 Hz and 2,000-5,000 Hz.
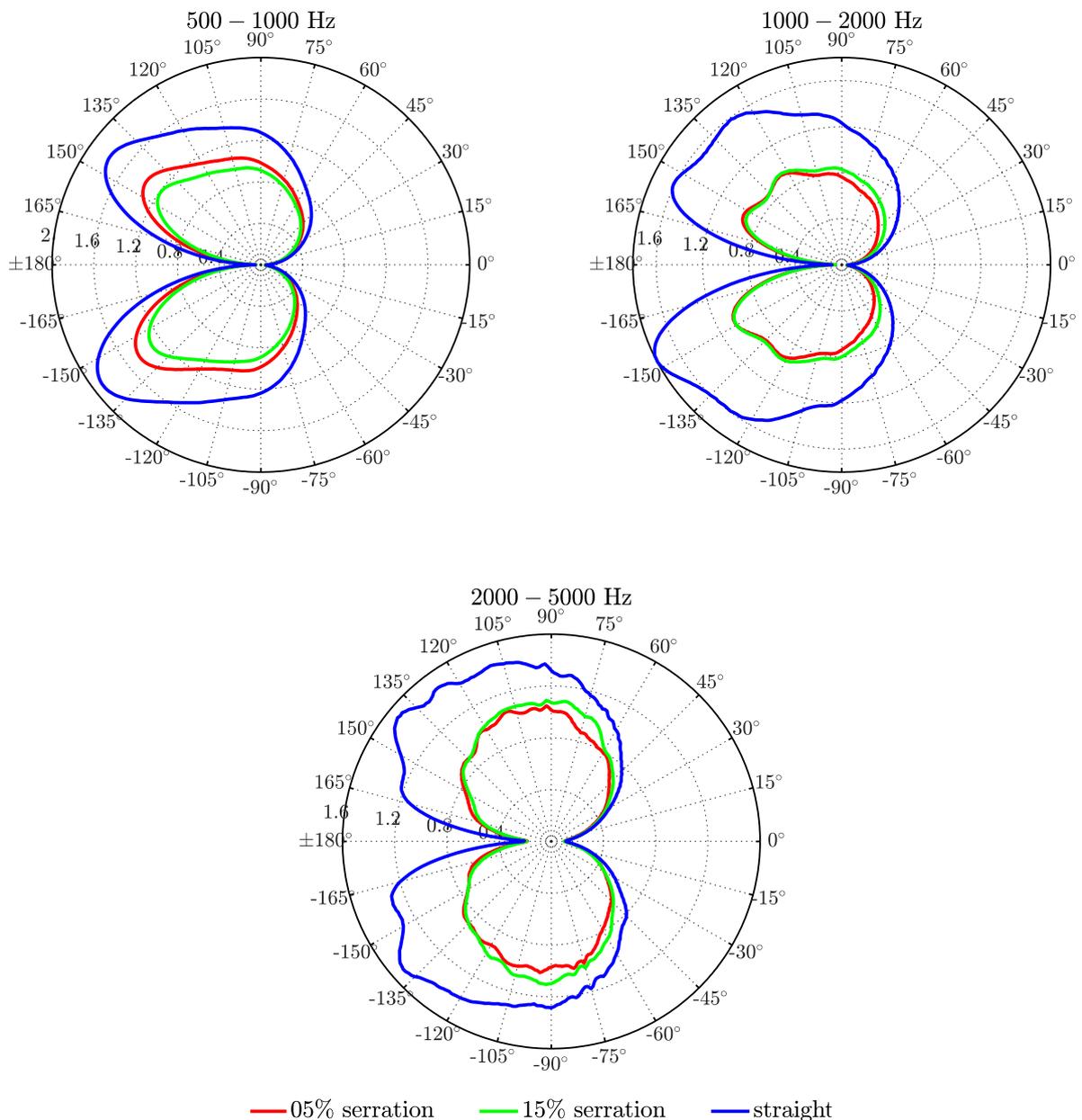
Figure 10 – Directivity plots for 500-1000 Hz (left), 1000-2000 Hz (right) and 2000-5000 Hz (bottom) for the baseline configuration and both serration cases for $\alpha = -2°$ and U = 37.4 m/s. The radial magnitude is the raw far-field pressure normalized by the baseline configuration.

In general, it can be observed that both serrated geometries provide considerable noise reductions at all angles, especially in the upstream direction (120-150⁰). The pattern of the directivity exhibits a convective dipole, oriented towards the leading edge. This is in line with diffraction pattern of trailing-edge noise cases. At the highest frequency band, lobes start to appear, indicating the change from compact to non-compact acoustic sources.

5.   Conclusions

Acoustic beamforming and computational simulations using the Lattice Boltzmann Method are used to investigate the noise emissions of a DU96-W-180 wind turbine profile. Two different trailing-edge serration geometries are studied and compared with the straight trailing-edge case (baseline). Both serrations are set at a flap angle of 6 degrees. The experimental campaign was performed in a closed-section wind tunnel with a microphone array and chord-based Reynolds numbers up to 1.5×10^6. The experimental trailing-edge noise spectra integrated over an area were compared with the simulations results, showing a satisfactory agreement between both and noise reductions up to 5 dB for the lower frequencies. A slight increase in noise is observed after a crossover frequency, which is supposed to be due to the serrations flap angle. The radiation directivity plots show a more dipole-like pattern for the serrated cases and a larger noise reduction in the upwind direction. This contribution also serves as a cross validation of both experimental and numerical approaches.

References

Arce León, C., Merino-Martinez, R., Ragni, D., Avallone, F. and Snellen, M. (2016a) *Boundary layer characterization and acoustic measurements of flow-aligned trailing edge serrations.* Experiments in Fluids 57(12):182. DOI: 10.1007/s00348-016-2272-z.

Arce León, C., Merino-Martinez, R., Ragni, D., Avallone, F. , Scarano, F., Pröbsting, S., Snellen, M., Simons, D.G. and Madsen, J. (2016b) *Effect of trailing edge serration-flow misalignment on airfoil noise emissions.* Journal of Sound and Vibration. Accepted for publication.

Avallone, F., Pröbsting, S. and Ragni D. (2016). *Three-dimensional flow field over a trailing-edge serration and implications on broadband noise.* Physics of Fluids 28:117101. DOI: 10.1063/1.4966633.

Bhatnagar, P., Gross, E. and Krook, M. (1954) *A model for collision processes in gases. Small amplitude processes in charged and neutral one-component systems.* Physical Review 94(3), 511-525. DOI: 10.1103/PhysRev.94.511.

Brandt, A. (2011) *Noise and vibration analysis: signal analysis and experimental procedures.* 2nd Edition. Wiley, Hoboken. ISBN 978-0-470-74644-8

Brès, G., Pérot, F. and Freed, D. (2010) *A Ffowcs Williams-Hawkings Solver for Lattice-Boltzmann Based Computational Aeroacoustics*, 16th AIAA/CEAS Aeroacoustics Conference, AIAA-2010-3711. DOI: 10.2514/6.2010-3711

Brooks, T. and Humphreys, W. (2006) *A deconvolution approach for the mapping of acoustic sources (DAMAS) determined from phased microphone arrays*. Journal of Sound and Vibration, Vol. 294. Nos. 4-5, 2016, pp 856-879. DOI: 10.1016/j.jsv.2005.12.046.

Chen, S. and Doolen, G. (1998) *Lattice Boltzmann method for fluid flows* Annual Review of Fluid Mechanics 30, 329-364.

Chen, H., Kandasamy, S., Orszag, S., Shock, R., Succi, S. and Yakhot, V. (2003) *Extended Boltzmann Kinetic Equation for Turbulent Flows*, Science (80-.). 301. 633–636. DOI: 10.1126/science.1085048.

Devenport, W., Burdisso, R.A., Camargo, H., Crede, E., Remillieux, M., Rasnick, M. and Van Seeters, P. (2010) *Aeroacoustic testing of wind turbine airfoils*. Virginia Polytechnic Institute and State University Blacksburg, Virginia, USA. May 2010. NREL/SR-500-43471.

Farassat, F., Succi, G.P. (1980) *A review of propeller discrete frequency noise prediction technology with emphasis on two current methods for time domain calculations*, Journal of Sound and Vibration 71, 399–419. DOI: 10.1016/0022-460X(80)90422-8.

Gruber, M., Joseph, P. and Chong, T. (2011) *On the mechanisms of serrated airfoil trailing edge noise reduction*. 17th AIAA/CEAS Aeroacoustics Conference, Portland, Oregon, USA. DOI: 10.2514/6.2011-2781.

Habibi, K., Gong, H., Nayafiyazdi, A. and Mongeau, L.G. (2013) *Prediction of the Sound radiated from Low-Mach Internal Mixing Nozzles with Forced Mixers using the Lattice Boltzmann Method.* 19th AIAA/CEAS Aeroacoustics Conference, Berlin, Germany: pp. 1–15. DOI: 10.2514/6.2013-2143.

Johnson, D.H. and Dudgeon D.E. (1993) *Array signal processing. Concepts and techniques.* PTR Prentice Hall. Englewood Cliffs. ISBN: 978-0-130-48513-7.

Malgoezar, A.M.N., Snellen, M., Merino-Martinez, R., Simons, D.G. and Sijtsma, P. (2017) On the use of global optimization methods for acoustic source mapping. Journal of the Acoustical Society of America. Vol. 141 No. 1. pp. 453-465. DOI: 10.1121/1.4973915.

Merino-Martinez, R., Snellen, M. and Simons, D.G. (2006) *Functional beamforming applied to imaging of flyover noise on landing aircraft*. Journal of Aircraft, Vol. 53 No. 6. pp. 1830-1843. DOI: 10.2514/1.C033691.

Mueller, T. (2002) *Aeroacoustic measurements*. Springer, Berlin. ISBN-978-3-642-07514-8.
Oerlemans, S. and Sijtsma, P. (2004) *Acoustic array measurements of a 1:10.6 scaled Airbus A340 model*. 10th AIAA/CEAS Aeroacoustics Conference, Manchester, United Kingdom. DOI: 10.2514/6.2004-2924.

Oerlemans, S., Fisher, M., Maeder, T. and Kögler, K. (2009) *Reduction of wind turbine noise using optimized airfoils and trailing-edge serrations.* AIAA Journal, Vol. 47, No. 6. 1470 – 1481. DOI: 10.2514/1.38888.

Oerlemans, S. and Fuglsang, P. (2012) *Low-noise wind turbine design* EWEA Workshop Oxford Palumbo, D (2012) Determining correlation and coherence lengths in turbulent boundary layer flight data Journal of Sound and Vibration 331(16), 3721-3737.

Oerlemans, S. (2016) Reduction of wind turbine noise using blade trailing edge devices. 22nd AIAA/CEAS Aeroacoustics Conference. May 30 – June 1 2016. Lyon, France. DOI: 10.2514/6.2016-3018.

Pagani, C.C.Jr., Souza, D.S. and Medeiros, M.A.F. (2016) *Slat noise: Aeroacoustic beamforming in closed-section wind tunnel with numerical comparison*. AIAA Journal 54 (7) 2100 – 2115. DOI: 10.2514/1.J054042.

Sarradj, E., Herold, G., Sijtsma, P., Merino-Martinez, R., Geyer, T.F., Bahr, C.J., Porteus, R., Moreau, D.J. and Doolan C.J. (2017) *A microphone array method benchmarking exercise using synthesized input data*. 23rd AIAA/CEAS Aeroacoustics Conference. June 5-9 2017. Denver, CO, USA. (Paper accepted for the conference).

Sijtsma, P. and Stoker, R.W. (2004) *Determination of absolute contributions of aircraft noise components using fly-over array measurements*. 10th AIAA/CEAS Aeroacoustics Conference. May 10 – 12 2004. Manchester, United Kingdom. DOI: 10.2514/6.2004-2958.

Sijtsma, P. (2010) *Phased array beamforming applied to wind tunnel and flyover tests*. Tech. Rep. NLR-TP-2010-549, National Aerospace Laboratory (NLR), The Netherlands (December 2010).

Sijtsma, P. (2016) *Analytical Benchmark 1*. 22nd AIAA/CEAS Aeroacoustics Conference. May 30 – June 1 2016. Lyon, France. Presentation in Microphone Array Methods Discussion Panel.

Succi, S. (2001) *The lattice Boltzmann equation for fluid dynamics and beyond*. 1st edition. Clarendon Press, Oxford.

Tuinstra, M. and Sijtsma, P. (2015) *Suppression of spurious noise sources in airfoil self-noise measurements*. 21st AIAA/CEAS Aeroacoustics Conference. June 22 – 26 2015. Dallas, TX, USA. DOI: 10.2514/6.2015-2689.

van der Velden, W.C.P., Pröbsting, S., van Zuijlen, A.H., de Jong, A.T., Guan, Y. and Morris, S.C. (2016) *Numerical and experimental investigation of a beveled trailing edge flow and noise field*. Journal of Sound and Vibration, 384 (2016) 113–129. DOI: 10.1016/j.jsv.2016.08.005.

van der Velden, W.C.P. and Oerlemans S. (2017) *Numerical analysis of noise reduction mechanisms on improved trailing edge serrations using the Lattice Boltzmann method*. 35th Wind Energy Symposium (AIAA SciTech Forum) January 9 – 13 2017. Grapevine, Texas, USA. DOI: 10.2514/6.2017-1379.

Westerweel, J. (1997) *Fundamentals of digital particle image velocimetry.* Measurement Science and Technology. 8, 1379–1392. DOI: 10.1088/0957-0233/8/12/002.

Williams, J.E.F., Hawkings, D.L. (1969) *Sound Generation by Turbulence and Surfaces in Arbitrary Motion*. Philos. Trans. R. Soc. London A Math. Phys. Eng. Sci. 264. DOI: 10.1098/rsta.1969.0031.

Yardibi, T., Li, J., Stoica, P., Zawodny, N. S. and Cattafesta III L. N. (2010) A covariance fitting approach for correlated acoustic source mapping. Journal of the Acoustic Society of America 127(5): 2920 – 2931. DOI: 10.1121/1.3365260.